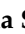








Communication

# New High Light Yield and Fast Ceramic Scintillator $\text{Y}_3\text{Al}_{2.5}\text{Ga}_{2.5}\text{O}_{12}:\text{Ce}$ , Mg

Valentina Smyslova <sup>1</sup>, Aliaksei Bondarau <sup>2</sup>, Andrei Fedorov <sup>1,3</sup>, Elizaveta Borisevich <sup>3</sup>, Ilya Lagutskiy <sup>4</sup>, Petr Karpuyk <sup>1</sup>, Ilia Komendo <sup>1,5</sup>, Vladimir Kalinov <sup>6</sup>, Vitaly Mechinsky <sup>1,3</sup>, Vasilii Retivov <sup>1</sup>, Yauheni Talochko <sup>7</sup>, Andrei Vasil'ev <sup>8</sup> and Mikhail Korzhik <sup>1,3,\*</sup>

- <sup>1</sup> National Research Center “Kurchatov Institute”, 123182 Moscow, Russia; smyslovavg@gmail.com (V.S.); afedorov123@yahoo.com (A.F.); silancedie@mail.ru (P.K.); komendo\_iyu@nrcki.ru (I.K.); vitaly.mechinsky@gmail.com (V.M.); vasilii\_retivov@mail.ru (V.R.)
- <sup>2</sup> Radiation Instruments and New Components LLC, 220600 Minsk, Belarus; alesonep@gmail.com
- <sup>3</sup> Institute for Nuclear Problems, Belarus State University, 220030 Minsk, Belarus; gapovaknopka@mail.ru
- <sup>4</sup> ATOMTEX SPE, 220005 Minsk, Belarus; lagutskiy\_ia@atomtex.com
- <sup>5</sup> Crystal Growth, Mendeleev University of Chemical Technology of Russia, 125047 Moscow, Russia
- <sup>6</sup> B.I. Stepanov Institute of Physics, National Academy of Sciences, 220072 Minsk, Belarus; v.kalinov@ifanbel.bas-net.by
- <sup>7</sup> Joint Institute for Nuclear Research, 141980 Dubna, Russia; yauheni.talochka@gmail.com
- <sup>8</sup> Scobel'tshin Institute of Nuclear Physics, Moscow State University, 119234 Moscow, Russia; anvasiliev52@gmail.com
- \* Correspondence: korjikmikhail@gmail.com

## Abstract

New scintillation transparent ceramics  $\text{Y}_3\text{Al}_{2.5}\text{Ga}_{2.5}\text{O}_{12}:\text{Ce}$ , Mg has been produced and evaluated for the first time. The material possesses a density of 5.17 g/cm<sup>3</sup>, a highlight yield of 44,000 ph/MeV, and an effective scintillation kinetics decay constant of 47 ns. This unique combination of the parameters makes it superior to YAG:Ce. Production of the material does not include tooling from precious materials, and the rate of the crystalline mass production is not limited by the pulling rate of the crystal growth process. It can be quite prospective to upgrade the detection units of a variety of X-ray imaging devices. The mechanism of the scintillation light yield enhancement and kinetics shortening in the material are discussed as well.

**Keywords:** scintillator; garnet structure; ceramics; light yield; scintillation kinetics



Received: 30 May 2025

Revised: 3 July 2025

Accepted: 3 July 2025

Published: 6 July 2025

**Citation:** Smyslova, V.; Bondarau, A.; Fedorov, A.; Borisevich, E.; Lagutskiy, I.; Karpuyk, P.; Komendo, I.; Kalinov, V.; Mechinsky, V.; Retivov, V.; et al. New High Light Yield and Fast Ceramic Scintillator  $\text{Y}_3\text{Al}_{2.5}\text{Ga}_{2.5}\text{O}_{12}:\text{Ce}$ , Mg. *Photonics* **2025**, *12*, 680. <https://doi.org/10.3390/photonics12070680>

**Copyright:** © 2025 by the authors. Licensee MDPI, Basel, Switzerland. This article is an open access article distributed under the terms and conditions of the Creative Commons Attribution (CC BY) license (<https://creativecommons.org/licenses/by/4.0/>).

## 1. Introduction

The yttrium aluminum garnet ( $\text{Y}_3\text{Al}_5\text{O}_{12}$ , YAG) scintillator activated by Ce has played an outstanding role in the detection technology of X-ray and gamma quanta since its discovery [1]. The material belongs to the cubic syngony; therefore, it can be produced in various ways in the form of single crystals, ceramics, or films [2–9]. Yttrium-aluminum garnet is tolerant to irradiation [10] and can be used in intense fields of ionizing radiation from gamma quanta and charged particles. At the same time, starting from the first systematic studies of this material [11,12], it was stated that the scintillation kinetics is relatively long, with a decay constant of ~100 ns [13,14]. Nowadays, the scintillation yield of YAG has been increased to ~35,000 ph/MeV by doping the crystal with  $\text{Mg}^{2+}$  ions. However, the decay constant was not reduced to less than 80 ns [15]. Currently, the material is produced by several manufacturers; the scintillation yield is declared to be 30,000–35,000 ph/MeV, and the decay constant of the kinetics is 70 ns [16,17]. Gd-less mixed garnet crystals typically

show similar results to YAG in LY [18,19]. The scintillation material  $(\text{Gd,Y})_3\text{Al}_2\text{Ga}_3\text{O}_{12}:\text{Ce}$ , Mg (GYAGG), having the scintillation yield of 50,000 ph/MeV and scintillation kinetics with a decay constant of 50 ns [20], could be considered as an alternative to YAG. A decrease in the gadolinium concentration in the compound also leads to a shift in the luminescence maximum to the short-wavelength spectral region in accordance with the results of [21]. However, in comparison with YAG, it has an increased density (5.86 versus 4.55 g/cm<sup>3</sup>). The material contains heavy Gd cations, which makes the material less suitable for recording soft X-rays in the energy range of less than 20 keV. Complete exclusion of gadolinium ions from the matrix was considered by the authors [22–24]. The scintillation yield of  $20,200 \pm 1000$  ph/MeV and the major component of the kinetics of 45 ns were obtained for the  $\text{YLu}_2\text{Al}_2\text{Ga}_3\text{O}_{12}$  material. On the other hand, a light yield of 23,500 photons/MeV and the major component of the kinetics of 54 ns were obtained when the  $\text{Lu}_2\text{YAl}_{2.5}\text{Ga}_{2.5}\text{O}_{12}:\text{Ce}$ , 0.05% Mg ceramics were produced. Spectacular results have been obtained with gadolinium-yttrium ceramics of the composition  $\text{Ce}:\text{Gd}_2\text{YGa}_3\text{Al}_2\text{O}_{12}$ ; the light yield is  $\sim 37,500$  ph/MeV, and the fast scintillation decay is 61 ns. The increased scintillation yield in GYAGG was achieved due to the combining of two factors. First, the dilution of the gadolinium subsystem in the crystal lattice, which increases the role of the exchange interaction in the transfer of electronic excitations to the activator ions. Then, the modulation of the conduction band bottom by compositional disordering of the matrix [25]. The greatest modulation effect from disordering is observed at mixing of Al and Ga ions in the crystal lattice of garnets made of trivalent cations [26]. Moreover, in the absence of gadolinium ions in the matrix, a change in the Ga and Al ratio in  $\text{Y}_3(\text{Al,Ga})_5\text{O}_{12}:\text{Ce}$  can shift the levels of the mixed  $4f^05d^{1-5}$  states. Therefore, the resonance conditions between the radiative transitions of STE [27] and the Stark components of the mixed configuration of  $\text{Ce}^{3+}$  ions might be obtained more accurately.

The procedure for how the Al/Ga ratio is technologically varied during sample production becomes a major factor as well. Ga ions are predominantly localized in tetrahedra and Al ions in octahedra in the garnet crystalline system consisting of trivalent cations. A change in their ratio in the raw material to produce the crystalline mass with a different Al/Ga ratio should be accompanied by the introduction of appropriate corrections to the cation composition. A defect formation is initiated in the matrix without composition correction, leading to deterioration of the user's parameters, in particular, the scintillation yield and a slowing down in the scintillation kinetics. Taking the above said into account, we have obtained transparent samples of scintillation ceramics of the compositions  $\text{Y}_3\text{Al}_{2.5}\text{Ga}_{2.5}\text{O}_{12}:\text{Ce}$  and  $\text{Y}_3\text{Al}_{2.5}\text{Ga}_{2.5}\text{O}_{12}:\text{Ce}$ , Mg. Their scintillation properties were evaluated. The possibilities of further improving the scintillation properties of the compound have been modeled and considered.

## 2. Materials and Methods

The precursor to produce ceramics was synthesized using the precipitator  $\text{NH}_4\text{HCO}_3$  with an excess of 30%. All chemicals used for coprecipitation had purity not worth that 5 N. A slight excess of yttrium (3.35 at.%) was introduced into the composition, which helps to accelerate the process of formation of transparent ceramics and also to correct the imbalance of the composition for other cations. The authors of [28] concluded that the gadolinium excess in the samples obtained by the ceramic method has a positive effect on the change in the scintillation yield. The excess gadolinium ions can be localized in octahedra in the garnet structure. Yttrium  $\text{Y}^{3+}$  has a smaller ionic radius in relation to  $\text{Gd}^{3+}$  when localized in the octahedron, 0.09 and 0.098 nm, respectively. Therefore, with an excess of yttrium in the precursor for the synthesis of ceramics, its ions can be localized with a higher probability in octahedra than gadolinium ions. When the Al/Ga ratio is shifted towards increasing the

Al content, some excess of Al ions will be created, which are predominantly localized in octahedra in aluminum-gallium garnet. The excess of Al ions compensates for the deficiency of gallium ions, predominantly localized in tetrahedrons, and yttrium ions compensate for vacancies in the octahedra. This reduces the possibilities for the formation of anion vacancies and color centers based on them, respectively. The precursor was heat-treated at 850 °C and ground in a PM-100 planetary mill, Retsch. Powders dried at a temperature of 70 °C were compacted by uniaxial pressing with a pressure of 250 MPa. Compacts were sintered in an RHTH80-300/18 Nabertherm furnace at a temperature of 1720 °C for 2 h in the oxide atmosphere. Samples of  $\text{Y}_{2.99}\text{Ce}_{0.01}\text{Al}_{2.5}\text{Ga}_{2.5}\text{O}_{12}$  (designation YG25-1.1) and  $\text{Y}_{2.99}\text{Ce}_{0.01}\text{Al}_{2.5}\text{Ga}_{2.5}\text{O}_{12} + \text{MgO}$  (50 ppm) (designation YG25-2.1) were produced. A commercially available YAG:Ce single crystal sample was used for comparison at PL and PLE measurements. The phase homogeneity of the samples was established by X-ray diffraction analysis using a Phaser D2, Bruker. The corresponding diffraction patterns are shown in Figure 1. The lattice parameters and crystal densities of the samples were calculated using the Rietveld method; the data are given in Table 1.

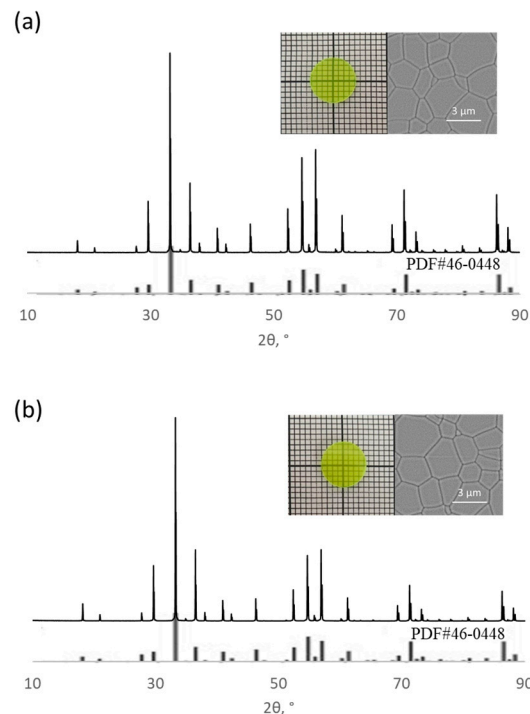


**Figure 1.** XRD patterns of the samples: (a) YG25-1.1; (b) YG25-2.1.

**Table 1.** Lattice parameters and crystal densities of YAGG:Ce ceramic samples.

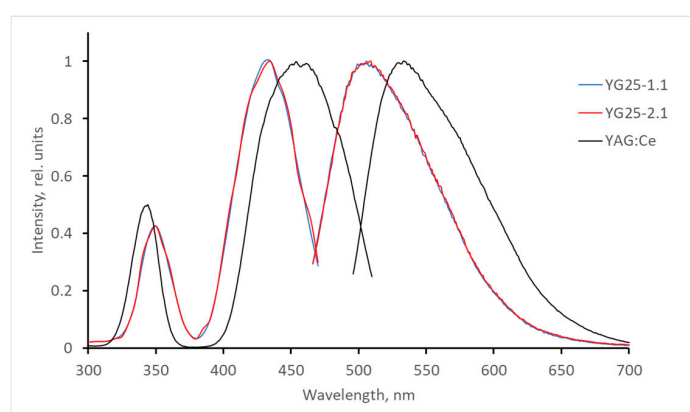
Sample	Rietveld Factor	a, Å	$\rho$ , g/cm <sup>3</sup>
YG25-1.1	2.67	12.165	5.17
YG25-2.1	3.74	12.162	5.17

Insets in Figure 1 show SEM images of the typical ceramic samples. As seen, they have similar morphology. The average grain size ( $\mu\text{m}$ ) for YG25-1.1 and YG25-2.1 was calculated to be  $1.8 \pm 0.1$  and  $1.9 \pm 0.1$   $\mu\text{m}$ , respectively. The residual porosity was defined to be 0.08 and 0.1%. For spectroscopic and spectrometric measurements, the samples were polished on one side; the thickness of the samples was 1 mm. Photoluminescence (PL) and its excitation (PLE) spectra of the samples were recorded using a Fluorat-02-PANORAMA spectrofluorimeter. Photoluminescence decay kinetics were recorded using

a FluoTime 250 PicoQuant spectrofluorimeter upon pulsed LED excitation at 270 and 450 nm; the instrumental response function (IRF) ranged from 1.5 to 2 ns. The light yield (LY) was evaluated at room temperature by an R329 (Hamamatsu) photomultiplier (PMT) with an integration time of 7  $\mu$ s in comparison with a CsI(Tl) scintillator with a diameter of 25.4 and a height of 25.4 mm. The light yield of the reference sample was 54,000 ph/MeV. Scintillation kinetics was measured at room temperature by the method of delayed coincidences with Philips XP2020 PMT in both channels.

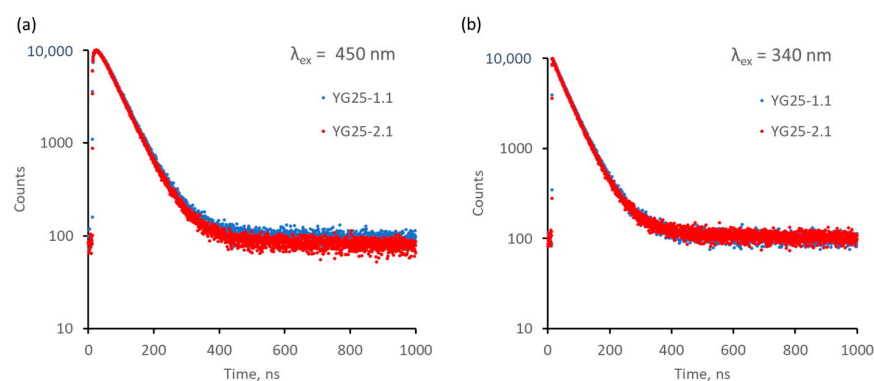
### 3. Results

Figure 2 shows the spectra of PL and PLE of the samples in comparison with YAG:Ce. It is evident that the luminescence spectra are significantly shifted to the short-wave region. Curves corresponding to YAGG:Ce and YAGG:Ce,Mg perfectly coincide, indicating an absence of the Mg codoping influence on the energies of the  $C^{3+}$  ions  $5d_{1,2}$  levels.



**Figure 2.** Luminescence and excitation spectra of samples in comparison with YAG:Ce spectra.

Figure 3 shows the photoluminescence kinetics curves of samples upon excitation of the  $4f^1 \rightarrow 4f^0 5d_1$  and  $4f_1 \rightarrow 4f^0 5d_2$  transitions, respectively. The PL decay constants are summarized in Table 2.



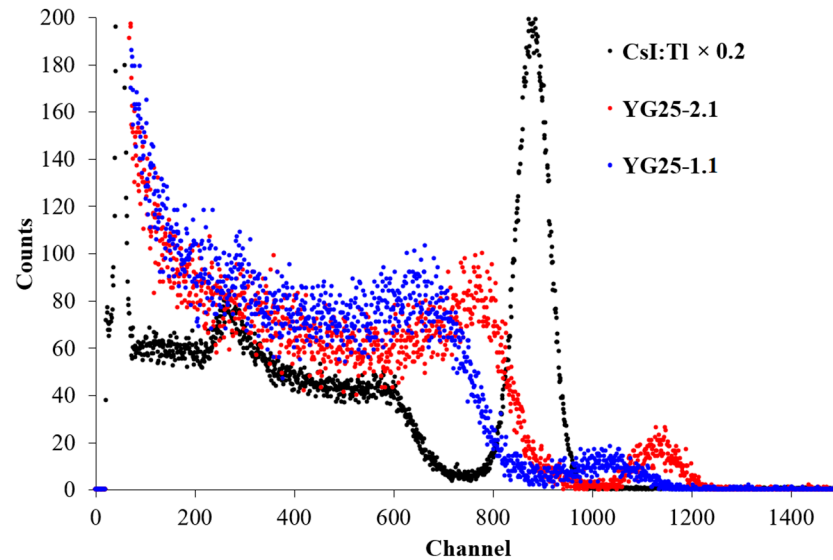
**Figure 3.** PL decay kinetics measured at room temperature. Samples and excitation wavelengths are imprinted in the pictures: (a)  $\lambda_{ex} = 340$  nm; (b)  $\lambda_{ex} = 450$  nm.

**Table 2.** Decay constants of the PL kinetics of the samples upon excitation of  $4f^0 5d_2$  and  $4f^0 5d_1$  levels of  $Ce^{3+}$  ions.

Sample	$\tau_1$ (Fraction), ns (%)	$\tau_2$ (Fraction), ns (%)	$\tau_1$ (Fraction), ns (%)
	$\lambda_{exc} 340$ nm	$\lambda_{exc} 340$ nm	$\lambda_{exc} 450$ nm
YG25-1.1	57 (91)	660 (4)	57 (100)
YG25-2.1	54 (96)	234 (3)	56 (100)

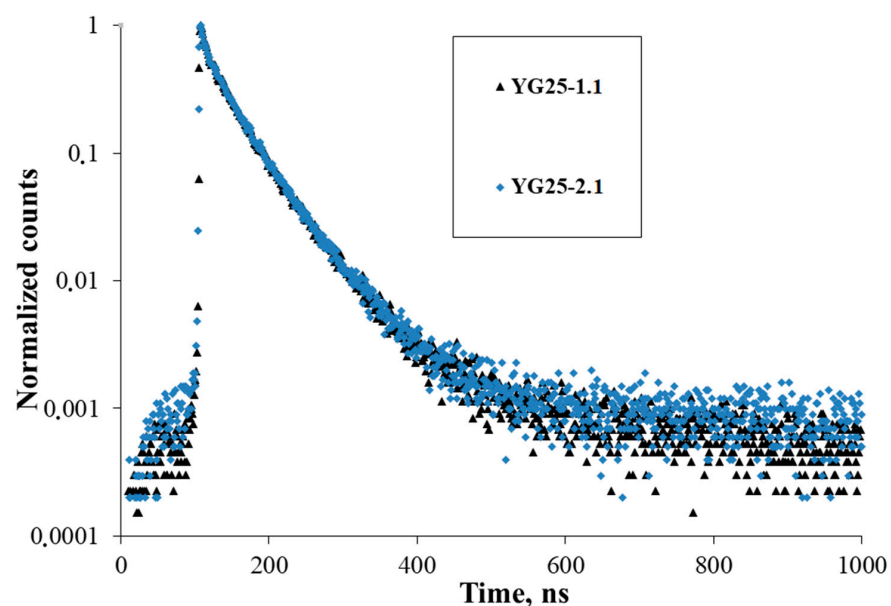
When exciting through the second Stark component of the  $4f^05d^1$  configuration, some fraction of the slow component is fitted at the approximation of the curves. It is typical for  $Ce^{3+}$  ions at the excitation in the levels located in the conduction zone of the compound.

Figure 4 shows the amplitude spectra of the  $^{137}\text{Cs}$  source of YAGG ceramic samples in comparison with the CsI(Tl) scintillator. Taking into account the spectral sensitivity of the PMT to the scintillation spectrum, the light output for the studied samples was defined as 39,500 (YG25-1.1) and  $43,000 \pm 1000$  ph/MeV (YG25-2.1).



**Figure 4.** Pulse height spectra of the  $^{137}\text{Cs}$  source measured with YAGG ceramic samples in comparison with the CsI(Tl) scintillator.

Figure 5 shows the scintillation kinetics of the samples. The kinetics are almost identical and are well approximated by two exponents with decay constants of 39 (85%) and 97 (15%) ns, while the effective decay time  $\langle \tau \rangle$  was estimated to be 47 ns. Note that the decay constant of the scintillation kinetics is less than that in the case of photoluminescence. This observation is not unique; a similar situation was observed in  $\text{LuAlO}_3:\text{Ce}$  [29].



**Figure 5.** Scintillation kinetics of YAGG:Ce and YAGG:Ce,Mg ceramic scintillator samples measured at room temperature.

Worth noting, the kinetics are preserved when codoped with magnesium, and the scintillation yield increases. This contrasts with the results in gadolinium-aluminum-gallium garnets [30] but correlates well with the results in gadolinium-free garnets [15].

#### 4. Discussion

The scintillation mechanism is based on the interaction of self-trapped excitons (STE) formed in the matrix and activator ions in oxygen compounds activated by  $\text{Ce}^{3+}$  ions, with no matrix-forming gadolinium ions [31]. Let us consider the positions of the maxima of the intrinsic luminescence bands in the matrices of the  $\text{Y}_3\text{Al}_5\text{O}_{12}$  and  $\text{Y}_3\text{Ga}_5\text{O}_{12}$  compounds having no compositional disorder. Their spectral maxima are summarized in Table 3. As a rule, the intrinsic luminescence in garnets consists of two broad luminescence bands localized in the UV region of the spectrum; designate them as the long-wave and short-wave bands. These bands have been studied for a long time in the yttrium and lutetium garnet compounds [32–36]. Gallium compounds with a garnet structure were evaluated for STE luminescence relatively recently [37]. The authors of [38] measured three bands of intrinsic luminescence at 4.13, 3.75, and 3.27 eV under laser excitation; the positions of the long-wave peaks correlate with the data of the above-mentioned references.

**Table 3.** Positions of the maxima of the intrinsic luminescence bands in  $\text{Y}_3\text{Al}_5\text{O}_{12}$  and  $\text{Y}_3\text{Ga}_5\text{O}_{12}$  compounds.

Compound	Short Wavelength Band, nm (eV)	Long Wavelength Band, nm (eV)	References
$\text{Y}_3\text{Al}_5\text{O}_{12}$	255 (4.9)	300 (4.2)	[31]
$\text{Y}_3\text{Ga}_5\text{O}_{12}$		325 (3.84)	[37]
		360 (3.47)	[37]
		302 (4.13)	[38]
		333 (3.75)	[38]
		382 (3.27)	[38]

As seen, the replacement of aluminum by gallium in the compound leads to a significant shift of the intrinsic luminescence bands to the long-wavelength region. In this case, a shift of the fundamental absorption edge from 6.4 to 5.86 eV also occurs. This happened due to the redistribution of the density of electron states in the conduction band. Moreover, the  $4f^05d^1$  radiative state of  $\text{Ce}^{3+}$  ions becomes localized in the conduction band. Hence, even when intrinsic luminescence in yttrium gallium garnet is quenched by  $\text{Ce}^{3+}$  impurity ions, their contribution to the scintillations or PL does not occur at room temperature. Therefore, the intrinsic luminescence is not detected in the studied compounds activated by cerium. It is obvious that a multiplicity of exciton states arises in aluminum gallium garnet. Due to compositional disordering, the STE states characteristic of both aluminum and gallium sublattices will be formed, as well as intermediate exciton states localized simultaneously near aluminum and gallium ions. Apparently, their energies will be lower than the STE energies in pure aluminum garnet; a shift towards lower energies with asymptotics to the STE energies in  $\text{Y}_3\text{Ga}_5\text{O}_{12}$  will be observed. At the same time, as seen from the spectroscopy data (Figure 2), upon transition from  $\text{Y}_3\text{Al}_5\text{O}_{12}$  to  $\text{Y}_3(\text{Al,Ga})_5\text{O}_{12}$ , a decrease in the energy of the electronic transition to the mixed  $4f^05d^2$  ( $\text{Ce}^{3+}$ ) state is observed. Its overlapping with the STE bands makes a significant contribution to the formation of scintillations. This ensures better resonance with the STE luminescence bands and, as a consequence, an increase in the scintillation yield. At the same time, this does not explain the almost 50% increase in the scintillation yield relative to  $\text{Y}_3\text{Al}_5\text{O}_{12}$  in  $\text{Y}_3(\text{Al}_{2.5}\text{Ga}_{2.5})_5\text{O}_{12}$ , as well as the increased yield in compounds with a ratio of  $\text{Al/Ga} = 1$  compared to  $\text{Al/Ga} = 2/3$ . Let us



analyze the change in the density of electronic states near the edges of the forbidden zone with a change in the Al/Ga ratio in the lattice. The density of states (DOS) was figured out using density functional theory (DFT) calculations of a cell containing 80 atoms, utilizing the Quantum Espresso package [39] in a nonrelativistic approximation using the Perdew–Burke–Eruzerhof (PBE) [40] exchange–correlation functional. In the unit cell of garnet, there are 8 octahedral positions and 12 tetrahedral positions. When changing the Al/Ga ratio in the lattice, it was assumed that gallium preferentially occupies tetrahedral positions. In this case, at a ratio of Al/Ga > 2/3, additional aluminum ions were randomly added to tetrahedral positions, and otherwise, gallium ions were added to octahedral positions. The calculation was performed for Al/Ga ratios equal to 5/0, 3.5/1.5, 2.5/2.5, 2/3, and 0/5. The calculation results are shown in Figure 6. It is known that the DFT method yields band gap values smaller than the experimental ones (by approximately 2.5 eV) due to incomplete consideration of correlation energies; however, the sequence of branches in the conduction and valence bands and their dispersions in the k-space are reproduced satisfactorily in these calculations.

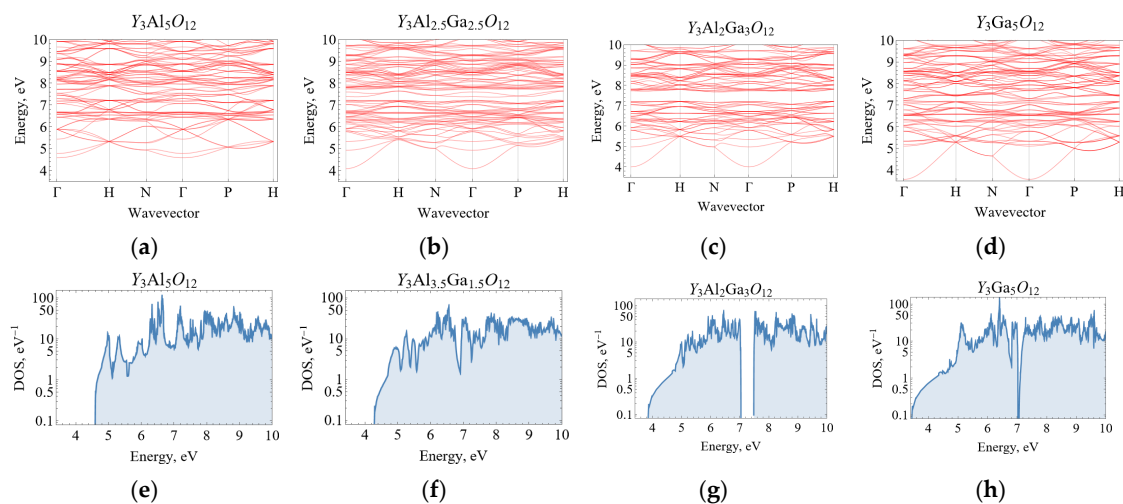


**Figure 6.** Results of DFT calculations of  $\text{Y}_3\text{Al}_{5-x}\text{Ga}_x\text{O}_{12}$  depending on the parameter  $x = 0, 2.5, 3, 5$ . Upper row: band structure of the lower part of the conduction band: (a)  $x = 0$ ; (b)  $x = 2.5$ ; (c)  $x = 3$ ; (d)  $x = 5$ . Lower row: density of states of the conduction band on a semi-logarithmic scale: (e)  $x = 0$ ; (f)  $x = 2.5$ ; (g)  $x = 3$ ; (h)  $x = 5$ .

Figure 6 shows the results of the DFT calculation of  $\text{Y}_3\text{Al}_{5-x}\text{Ga}_x\text{O}_{12}$  for the parameter  $x = 0, 2.5, 3$ , and 5. The energy is measured from the top of the valence band. The decomposition of DOS by elements shows that in YAG the bottom of the conduction band is almost completely formed by the 5d states of yttrium (with a small hybridization with the surrounding oxygen ions). However, in the presence of gallium, the situation changes significantly. A separate branch appears that splits off from the main group of branches of the conduction band. The appearance of this branch explains the long-wave shift of the STE luminescence bands upon transition from aluminum to gallium garnet. Yttrium and gallium make almost equal contributions to the formation of this branch. The effective mass of an electron on this lower branch of the conduction band systematically decreases with increasing the gallium concentration, which will provide a corresponding increase in the electron mobility and the separation of secondary electrons from the hole created simultaneously. This effect is of significant importance when assessing the electron escape from holes, since, despite the small contribution to the density of states (Figure 6e–h), all electrons undergo cooling along this branch during relaxation. Due to the low density of states on this branch, the phonon emission rate decreases. Hence, the electron cooling

rate and relaxation along this branch can significantly increase the electron escape at thermalization. Consequently, the probability of geminate pairs binding into excitons decreases, and the scintillation yield due to the interaction of STE and  $\text{Ce}^{3+}$  ions decreases. It is worth noting another feature of these compounds, which is most clearly manifested for the compound of the  $\text{Y}_3\text{Al}_2\text{Ga}_3\text{O}_{12}$  composition, namely, the appearance of a gap in the density of states at an energy 3 eV higher than the conduction band bottom. Analysis of the DOS distribution by elements shows that the states above this gap have a significantly higher contribution from the electronic states of gallium compared to the states below the gap. With increasing aluminum concentration, this gap, which is highest at the ratio  $\text{Ga}/\text{Al} = 3/2$ , decreases due to the splitting of the branches. The presence of such dips in the density of states affects the relaxation of secondary electrons created with energies above this gap. An estimation of the fraction of such electrons created by inelastic processes of electron-electron scattering and having kinetic energy larger than the bandgap by a factor of 3 gives a number  $\sim 20\text{--}30\%$ . Such electrons will relax in energy at a rate that has minimal values in the region of the dip, especially if one takes into account that the dip width for  $\text{Y}_3\text{Al}_2\text{Ga}_3\text{O}_{12}$  exceeds the energy of an optical phonon. Typically, it is  $\sim 100$  meV for oxide garnet structure materials. Thus, electrons with an initial energy above the dip will more actively escape from the place of their birth compared to electrons with energies below the gap.

## 5. Conclusions

The new scintillation material  $\text{Y}_3\text{Al}_{2.5}\text{Ga}_{2.5}\text{O}_{12}:\text{Ce}$ , Mg was produced in the form of transparent ceramics. It is characterized by a high scintillation yield of 44,000 ph/MeV and fast scintillation kinetics with an effective decay constant of 47 ns.

An increase in the scintillation yield of the compound is explained by the role of the Ga ions in the DOS forming. When gallium is introduced into the lattice, a branch is split off from the major group of conduction band branches in DOS. The appearance of this branch leads to a long-wave shift of the STE luminescence bands and their better resonance with the activator absorption bands and, consequently, to a more efficient transfer of electronic excitation energy to the activator ions. This also leads to an increase in the transfer rate and, as a consequence, to an acceleration of the scintillation kinetics. It is obvious that these effects are determined by the energy gap between the branch and the main group of states. Too large a gap, as in  $\text{Y}_3\text{Ga}_5\text{O}_{12}$ , on the contrary, leads to a decrease in the yield due to the detuning of resonance conditions.

The better yield of scintillations in relation to  $\text{Y}_3\text{Al}_2\text{Ga}_3\text{O}_{12}:\text{Ce}$  is explained by the appearance of a dip in the density of states at an energy 3 eV above the bottom of the conduction band. With increasing aluminum concentration, this gap is highest at a ratio of  $\text{Ga}/\text{Al} = 3/2$  and then decreases due to the splitting of branches. The presence of such dips in the density of states negatively affects the thermalization rate of secondary electrons created with energies above this gap.

Finally, the role of co-activating  $\text{Mg}^{2+}$  ions changes in the compound under consideration. It is known that in oxide compounds, coactivation by  $\text{Mg}^{2+}$  ions replacing trivalent cations in the lattice leads to the formation of a deep trapping center with fast nonradiative relaxation. In wide-gap oxygen compounds based on Al or Si, the exciton states have energies higher than the depth of such defects, which leads to quenching of their luminescence and, as a consequence, to a decrease in the scintillation yield. When the aluminum subsystem is diluted with gallium and a split-off branch is formed, the centers based on  $\text{Mg}^{2+}$  change their role from quenchers into donors of  $\text{Ce}^{3+}$  luminescence via interaction with STE, which explains the increase in the scintillation yield compared to a sample not coactivated with magnesium.



**Author Contributions:** Methodology, V.S.; Validation, V.R.; Formal analysis, Y.T.; Investigation, A.B., E.B., I.L., P.K. and V.M.; Data curation, A.F. and I.K.; Writing—original draft, M.K.; Writing—review & editing, A.V.; Visualization, V.K. All authors have read and agreed to the published version of the manuscript.

**Funding:** The research was supported by the Russian Science Foundation, grant No. 25-73-30014 <https://rscf.ru/en/project/25-73-30014/> (accessed 30 May 2025).

**Institutional Review Board Statement:** Not applicable.

**Informed Consent Statement:** Not applicable.

**Data Availability Statement:** All data are included in the article.

**Acknowledgments:** Research was conducted using equipment of the Research Chemical and Analytical Center NRC “Kurchatov Institute” Shared Research Facilities. The research is carried out using the equipment of the shared research facilities of HPC computing resources at Lomonosov Moscow State University.

**Conflicts of Interest:** Author Aliaksei Bondarau was employed by the company Radiation Instruments and New Components LLC. The remaining authors declare that the research was conducted in the absence of any commercial or financial relationships that could be construed as a potential conflict of interest.

## References

1. Autrata, R.; Schauer, P.; Kuapil, J.; Kuapil, J. A Single Crystal of YAG-New Fast Scintillator in SEM. *J. Phys. E* **1978**, *11*, 707. [CrossRef]
2. Greskovich, C.; Duclos, S. Ceramic scintillators. *Annu. Rev. Mater. Res.* **1997**, *27*, 69–88. [CrossRef]
3. Yanagida, T.; Takahashi, H.; Ito, T.; Kasama, D.; Enoto, T.; Sato, M.; Hirakuri, S.; Kokubun, M.; Makishima, K.; Yanagitani, T.; et al. Evaluation of Properties of YAG (Ce) Ceramic Scintillators. *IEEE Trans. Nucl. Sci.* **2005**, *52*, 1836–1841. [CrossRef]
4. Wang, X.; Dai, Y.; Zhang, Z.; Su, L.; Kou, H.; Wang, Y.; Wu, A. Optical and Scintillation Properties of Ce:Y<sub>3</sub>Al<sub>5</sub>O<sub>12</sub> Single Crystal Fibers Grown by Laser Heated Pedestal Growth Method. *J. Rare Earths* **2021**, *39*, 1533–1539. [CrossRef]
5. Kucera, M.; Nitsch, K.; Kubova, M.; Solovieva, N.; Nikl, M.; Mares, J.A. Ce-doped YAG and LuAG Epitaxial Films for Scintillation Detectors. *IEEE Trans. Nucl. Sci.* **2008**, *55*, 1201–1205. [CrossRef]
6. Zorenko, Y.; Mares, J.A.; Prusa, P.; Nikl, M.; Gorbenko, V.; Savchyn, V.; Kucerkova, R.; Nejezchleb, K. Luminescence and scintillation characteristics of YAG:Ce single crystalline films and single crystals. *Radiat. Meas.* **2010**, *45*, 389–391. [CrossRef]
7. Zorenko, Y.; Gorbenko, V.; Konstankevych, I.; Voloshinovskii, A.; Stryganyuk, G.; Mikhailin, V.; Kolobanov, V.; Spassky, D. Single-crystalline films of Ce-doped YAG and LuAG phosphors: Advantages over bulk crystals analogues. *J. Lumin.* **2005**, *114*, 85–94. [CrossRef]
8. Mares, J.A.; Nikl, M.; Beitlerova, A.; Horodysky, P.; Blazek, K.; Bartos, K.; D’Ambrosio, C. Scintillation Properties of Ce<sup>3+</sup>- and Pr<sup>3+</sup>-Doped LuAG, YAG and Mixed Lu<sub>x</sub>Y<sub>1-x</sub>AG Garnet Crystals. *IEEE Trans. Nucl. Sci.* **2012**, *59*, 2120–2125. [CrossRef]
9. Mihóková, E.; Nikl, M.; Mareš, J.A.; Beitlerová, A.; Vedda, A.; Nejezchleb, K.; Blažek, K.; D’Ambrosio, C. Luminescence and scintillation properties of YAG:Ce single crystal and optical ceramics. *J. Lumin.* **2007**, *126*, 77–80. [CrossRef]
10. Lucchini, M.T.; Pauwels, K.; Blazek, K.; Ochesanu, S.; Auffray, E. Radiation tolerance of LuAG:Ce and YAG:Ce crystals under high levels of gamma- and proton-irradiation. *IEEE Trans. Nucl. Sci.* **2016**, *63*, 586–590. [CrossRef]
11. Moszyński, M.; Ludziejewski, T.; Wolski, D.; Klamra, W.; Norlin, L.O. Properties of the YAG:Ce scintillator. *Nucl. Instrum. Methods Phys. Res. Sect. A Accel. Spectrometers Detect. Assoc. Equip.* **1994**, *345*, 461–467. [CrossRef]
12. Ludziejewski, T.; Moszyński, M.; Kapusta, M.; Wolski, D.; Klamra, W.; Moszyńska, K. Investigation of Some Scintillation Properties of YAG:Ce Crystals. *Nucl. Instrum. Methods Phys. Res. Sect. A Accel. Spectrometers Detect. Assoc. Equip.* **1997**, *398*, 287–294. [CrossRef]
13. Nikl, M. Scintillation detectors for x-rays. *Meas. Sci. Technol.* **2006**, *17*, R37–R54. [CrossRef]
14. Zych, E.; Brecher, C.; Glodo, J. Kinetics of cerium emission in a YAG:Ce single crystal: The role of traps. *J. Phys. Condens. Matter* **2000**, *12*, 1947–1958. [CrossRef]
15. Zapadlík, O.; Nikl, M.; Polák, J.; Průša, P.; Linhart, V. Engineering of YAG:Ce to improve its scintillation properties. *Opt. Mater. X* **2022**, *15*, 100165. [CrossRef]
16. Advatech-UK. Available online: [https://www.advatech-uk.co.uk/yag\\_ce.html](https://www.advatech-uk.co.uk/yag_ce.html) (accessed on 5 April 2025).

17. Crytur. Available online: <https://www.crytur.cz/materials/yagce/> (accessed on 5 April 2025).
18. Sreebunpeng, K.; Chewpraditkul, W.; Chewpraditkul, W.; Kucerkova, R.; Beitlerova, A.; Nikl, V.; Szczesniak, T.; Grodzicka-Kobylka, M.; Zhu, D.; Hu, C.; et al. Luminescence and scintillation properties of fast Ce,Mg:Lu<sub>2</sub>YGa<sub>x</sub>Al<sub>5-x</sub>O<sub>12</sub> ceramic scintillators fabricated from co-precipitated powders. *Opt. Mater.* **2024**, *152*, 115418. [\[CrossRef\]](#)
19. Chewpraditkul, W.; Pattanaboonmee, N.; Chewpraditkul, W.; Kamada, K.; Kim, K.-J.; Yoshikawa, A.; Makowski, M.; Witkowski, V.; Drozdowski, W.; Beitlerova, A.; et al. Optical and scintillation characteristics of Lu<sub>2</sub>Y(Al<sub>5-x</sub>Ga<sub>x</sub>)O<sub>12</sub>:Ce,Mg multicomponent garnet crystals. *Opt. Mater.* **2022**, *134*, 113186. [\[CrossRef\]](#)
20. Korzhik, M.; Alenkov, V.; Buzanov, O.; Dosovitskiy, G.; Fedorov, A.; Kozlov, D.; Mechinsky, V.; Nargelas, S.; Tamulaitis, G.; Vaitkevičius, A. Engineering of a new single-crystal multi-ionic fast and high-light-yield scintillation material (Gd<sub>0.5</sub>-Y<sub>0.5</sub>)<sub>3</sub>Al<sub>2</sub>Ga<sub>3</sub>O<sub>12</sub>:Ce,Mg. *CrystEngComm* **2020**, *22*, 2502–2506. [\[CrossRef\]](#)
21. Ueda, J.; Tanabe, S. (INVITED) Review of luminescent properties of Ce<sup>3+</sup>-doped garnet phosphors: New insight into the effect of crystal and electronic structure. *Opt. Mater. X* **2019**, *1*, 100018. [\[CrossRef\]](#)
22. Chewpraditkul, W.; Pattanaboonmee, N.; Chewpraditkul, W.; Szczesniak, T.; Moszynski, M.; Kamada, K.; Yoshikawa, A.; Kucerkova, R.; Nikl, M. Optical and scintillation properties of LuGd<sub>2</sub>Al<sub>2</sub>Ga<sub>3</sub>O<sub>12</sub>:Ce, Lu<sub>2</sub>GdAl<sub>2</sub>Ga<sub>3</sub>O<sub>12</sub>:Ce, and Lu<sub>2</sub>YAl<sub>2</sub>Ga<sub>3</sub>O<sub>12</sub>:Ce single crystals: A comparative study. *Nucl. Instrum. Methods Phys. Res. Sect. A Accel. Spectrometers Detect. Assoc. Equip.* **2021**, *1004*, 165381. [\[CrossRef\]](#)
23. Chewpraditkul, W.; Horiai, T.; Beitlerova, A.; Kucerkova, R.; Babin, V.; Yoshikawa, A.; Chewpraditkul, W.; Nikl, M. Temperature dependence of photo- and radio-luminescence and scintillation properties of Lu<sub>2</sub>YAl<sub>2.5</sub>Ga<sub>2.5</sub>O<sub>12</sub>:Ce,Mg multicomponent garnet crystals. *Opt. Mater.* **2024**, *147*, 114738. [\[CrossRef\]](#)
24. Chen, X.; Liu, X.; Feng, Y.; Li, X.; Chen, H.; Xie, T.; Kou, H.; Kučerková, R.; Beitlerová, A.; Mihóková, E.; et al. Microstructure evolution in two-step-sintering process toward transparent Ce:(Y,Gd)<sub>3</sub>(Ga,Al)<sub>5</sub>O<sub>12</sub> scintillation ceramics. *J. Alloys Compd.* **2020**, *846*, 156377. [\[CrossRef\]](#)
25. Smyslova, V.G.; Retivov, V.M.; Dubov, V.V.; Ermakova, L.V.; Ivanov, V.K.; Karpyuk, P.V.; Komendo, I.Y.; Lelekova, D.E.; Mechinsky, V.A.; Vasiliev, A.N.; et al. Effect of nanostructuring of coprecipitated precursors on the morphology and scintillation properties of multication ceramics with a garnet structure. *Nanosyst. Phys. Chem. Math.* **2024**, *15*, 2220–8054. [\[CrossRef\]](#)
26. Korzhik, M.; Retivov, V.; Dubov, V.; Ivanov, V.; Komendo, I.; Lelekova, D.; Karpyuk, P.; Mechinsky, V.; Postupaeva, A.; Smyslova, V.; et al. Compositional disordering: Nanoscale engineering of advanced crystalline scintillation materials. *J. Appl. Phys.* **2024**, *135*, 0021–8979. [\[CrossRef\]](#)
27. Korzhik, M.; Tamulaitis, G.; Vasil'ev, A.N. *Physics of Fast Processes in Scintillators*; Particle Acceleration and Detection; Springer International Publishing: Cham, Switzerland, 2020.
28. Retivov, V.; Dubov, V.; Kuznetsova, D.; Ismagulov, A.; Korzhik, M. Gd<sup>3+</sup> content optimization for mastering high light yield and fast Gd<sub>x</sub>Al<sub>2</sub>Ga<sub>3</sub>O<sub>12</sub>:Ce<sup>3+</sup> scintillation ceramics. *J. Rare Earths* **2022**, *41*, 1911–1918. [\[CrossRef\]](#)
29. Moses, W.W.; Derenzo, S.E.; Fyodorov, A.; Korzhik, M.; Gektin, A.; Minkov, B.; Aslanov, V. LuAlO<sub>3</sub>:Ce—a high density, high speed scintillator for gamma detection. *IEEE Trans. Nucl. Sci.* **1995**, *42*, 275–279. [\[CrossRef\]](#)
30. Nargelas, S.; Solovjovas, A.; Talochka, Y.; Podlipskas, Ž.; Kucera, M.; Lucenicova, Z.; Tamulaitis, G. Influence of heavy magnesium codoping on emission decay in Ce-doped multicomponent garnet scintillators. *J. Mater. Chem. C* **2023**, *11*, 12007–12015. [\[CrossRef\]](#)
31. Korzhik, M.V.; Trower, W.P. Origin of scintillation in cerium\_doped oxide crystals. *Appl. Phys. Lett.* **1995**, *66*, 2327. [\[CrossRef\]](#)
32. Hayes, W.; Yamaga, M.; Robbins, D.J.; Cocklane, B. Optical detection of excitation EPR in LiYF<sub>4</sub>. *Solid-State Phys.* **1980**, *13*, L1085. [\[CrossRef\]](#)
33. Kuznetsov, A.I.; Namosov, B.R.; Murk, V.V. Relaxed electronic states in Al<sub>2</sub>O<sub>3</sub>, Y<sub>3</sub>Al<sub>5</sub>O<sub>12</sub>, YAlO<sub>3</sub>. *Solid State Phys (USSR)* **1985**, *27*, 3030–3035.
34. Kuznetsov, A.I.; Abramov, V.N.; Murk, V.V.; Namosov, B.R. States of the self-trapped excitons in complex oxides. *Sov. Phys. Solid State* **1991**, *33*, 2000–2004.
35. Wood, R.L.; Hayes, W. A study of recombination centres in YAlO<sub>3</sub>, EuAlO<sub>3</sub>, LaAlO<sub>3</sub> and Y<sub>2</sub>O<sub>3</sub> using ODMR. *Radiat. Eff.* **1983**, *72*, 195. [\[CrossRef\]](#)
36. Andriessen, J.; Dorenbos, P.; van Eijk, C.W.E. *Ce<sup>3+</sup> Doped Scintillation Materials. Scintillators and Phosphor Materials*; Weber, M.J., Lecoq, P., Ruchti, R.C., Woody, C., Yen, W.M., Zhu, R.-Y., Eds.; Material Research Society: Pittsburgh, PA, USA, 1994; p. 355.
37. Yamaji, A.; Yanagida, T.; Yokota, Y.; Fujimoto, Y.; Sugiyama, M.; Yoshikawa, A. Comparative study on scintillation properties of LGG, YGG and GGG. In Proceedings of the 2010 IEEE Nuclear Science Symposium, Medical Imaging Conference, Knoxville, TN, USA, 30 October–6 November 2010; pp. 179–181. [\[CrossRef\]](#)
38. Zorenko, Y.; Zorenko, T.; Vistovskyy, V.; Grinberg, M.; Łukasiewicz, T. Time-resolved spectroscopy of intrinsic luminescence of Y<sub>3</sub>Ga<sub>5</sub>O<sub>12</sub> and (LaLu)<sub>3</sub>Lu<sub>2</sub>Ga<sub>3</sub>O<sub>12</sub> single crystals. *Opt. Mater.* **2009**, *31*, 1835–1838. [\[CrossRef\]](#)

39. Giannozzi, P.; Baroni, S.; Bonini, N.; Calandra, M.; Car, R.; Cavazzoni, C.; Ceresoli, D.; Chiarotti, G.L.; Cococcioni, M.; Dabo, I. QUANTUM ESPRESSO: A modular and open-source software project for quantum simulations of materials. *J. Phys. Condens.* **2009**, *21*, 395502. [[CrossRef](#)]
40. Perdew, J.P.; Burke, K.; Ernzerhof, M. Generalized Gradient Approximation Made Simple. *Phys. Rev. Lett.* **1996**, *77*, 3865. [[CrossRef](#)]

**Disclaimer/Publisher's Note:** The statements, opinions and data contained in all publications are solely those of the individual author(s) and contributor(s) and not of MDPI and/or the editor(s). MDPI and/or the editor(s) disclaim responsibility for any injury to people or property resulting from any ideas, methods, instructions or products referred to in the content.